

1 **Revision 4**

2 **Sound velocities across calcite phase transitions by Brillouin**
3 **scattering spectroscopy**

4 Chao-shuai Zhao^{1,2}, He-ping Li^{1*}, Po-fei Chen³, Jian-jun Jiang¹

5 ¹*Key Laboratory of High-temperature and High-pressure Study of the Earth's Interior,*

6 *Institute of Geochemistry, Chinese Academy of Sciences, 550081 Guiyang, China*

7 ²*College of Earth Sciences, University of Chinese Academy of Sciences, 100049*

8 *Beijing, China*

9 ³*Department of Earth Sciences, National Central University, 32001 Taoyuan, Taiwan,*

10 *China*

11 **Abstract**

12 Calcite (CaCO₃) is widely considered an important carbon carrier in the Earth's
13 interior. Laboratory measurements of the velocities and elastic properties of calcite
14 are important for understanding the deep carbon cycle. The sound velocities of calcite
15 were determined up to 10.3 GPa at ambient temperature by Brillouin scattering
16 spectroscopy. Dramatic decreases in the velocity of compressional wave (V_p) and
17 shear wave (V_s) and abrupt increases in the V_p anisotropy (A_p) and maximum V_s
18 anisotropy (A_{max}) were detected across the phase transition from CaCO₃-I to
19 CaCO₃-II. Dramatic increases in the V_p and V_s and an abrupt decrease in A_p were
20 observed across the phase transition from CaCO₃-II to CaCO₃-III. The phase
21 transition from CaCO₃-I to CaCO₃-II may potentially explain the Gutenberg
22 discontinuity at 51 km in the Izu-Bonin region. The V_p and V_s values of calcite were
23 rather low. Our new results combined with literature data suggest that the rather low
24 velocities of CaCO₃ could potentially explain the low-velocity zone occurring in

*Corresponding author. Email: liheping@vip.gyig.ac.cn

25 northeastern (NE) Japan.

26 Keywords: Brillouin scattering; sound velocity; elasticity; CaCO₃; high-pressure.

27 **Introduction**

28 Carbonates play an important role in the transport and storage of carbon in the
29 Earth's crust and mantle (Dasgupta and Hirschmann 2010; Sanchez-Valle et al. 2011).
30 Calcite is widely considered one of the most important carbonates in the Earth's
31 interior. Recent experimental and theoretical studies have shown that its high-pressure
32 phase remains stable under lower mantle pressure and temperature conditions
33 (Dorfman et al. 2018; Liu et al. 2016; Oganov et al. 2006, 2008; Ono et al. 2007; Li et
34 al. 2018). The existence of calcite in the mantle is also proven by the occurrence of its
35 inclusion in diamonds at corresponding depths (Brenker et al. 2007; Kaminsky et al.
36 2009; Tschauer et al. 2018). Additionally, sound velocities and elastic properties are
37 important for understanding the structure of the Earth's interior and the causes of
38 some abnormal behaviors (e.g., seismic wave discontinuities and low-velocity zones)
39 (Mao et al. 2010; Duffy et al. 1995; Bayarjargal et al. 2018; Marcondes et al. 2016).
40 Laboratory measurements of the velocities and elastic properties of calcite are thus
41 important for determining the deep carbon cycle and identifying potential carbonate-
42 rich regions in the Earth's interior.

43 Calcite crystallizes in the trigonal crystal system with space group $R\bar{3}c$ (referred to
44 as CaCO₃-I) under ambient conditions. It undergoes a series of structural phase
45 transitions into CaCO₃-II, CaCO₃-III, and CaCO₃-VI at ~1.5, ~2.1, and ~15.0 GPa,
46 respectively (Catalli 2005; Liu et al. 2016; Merlini et al. 2012). There are numerous
47 experimental and theoretical reports on the velocity and elasticity of calcite. However,
48 these studies are mainly concentrated on low-pressure measurements with ultrasonic
49 interferometry or high-pressure conditions modeled through theoretical calculation

50 (Almqvist et al. 2010; Grady et al. 1978; Juneja and Endait 2017; Thanh and Lacam
51 1984; Peselnick and Robie 1963; Stekiel et al. 2017; Wang 1966; Zhao et al. 2009;
52 Huang et al. 2017; Bayarjargal et al. 2018). Furthermore, some data on properties at
53 ambient pressure and/or high-temperatures based on Brillouin scattering spectroscopy
54 have been reported (Chen et al. 2001; Lin 2013). Therefore, we investigated the high-
55 pressure velocities of natural calcite up to 10.3 GPa at ambient temperature by
56 Brillouin scattering spectroscopy.

57 **Methods**

58 Natural single-crystal calcite (Iceland spar) samples were obtained from Guizhou,
59 China. The composition was measured by electron microprobe analyses (JXA-8230,
60 15 kV and 10 nA, Northwest University, China), which indicated a homogeneous
61 chemical composition of CaCO₃ with less than 0.4 mol% Mg. For simplification, we
62 refer to it as CaCO₃. Single-crystal samples with optical clarity, surface smoothness,
63 and parallelism of less than 30' were chosen for Brillouin scattering measurements.

64 High-pressures were generated by a pair of 400 μm diamond culets. The sample
65 chamber was composed of a rhenium gasket with a pre-indented thickness of ~70 μm
66 and a drilled hole of ~160 μm. A volume ratio of 4:1 methanol and ethanol mixture
67 was applied as the pressure transmitting medium for all experiments. Ruby powders
68 and a single-crystal platelet with a thickness of ~40 μm were loaded into the sample
69 chamber. Four independent experiments were conducted in this study. Pressures were
70 determined by the quasi-hydrostatic ruby scale (Mao et al. 1986). The pressure
71 uncertainties were ±0.1 GPa below 2 GPa and ±0.3 GPa between 3 and 10.3 GPa,
72 which were estimated from the pressure measured before and after the collection of
73 the Brillouin spectra.

74 Brillouin scattering spectra were collected by a Sandercock-type six-pass tandem

75 Fabry-Perot interferometer (TFP-2, JRS Scientific Instruments) equipped with a phot-
76 omultiplier detector (Count-10B, Laser Components) and a diode-pumped laser with a
77 wavelength of 532 nm (Verdi G2, Coherent) as an excitation source. A 60° symmetric
78 scattering geometry was adopted in all experiments. The Brillouin scattering system
79 was calibrated before the measurements with BK7 glass and deionized water
80 (Sanchez-Valle et al. 2013; Yoneda and Song 2005). The aggregate velocities were
81 calculated as follows:

$$82 \quad V_i = \frac{\Delta\omega_i \lambda}{2 \sin(\theta/2)}, \quad (1)$$

83 where V_i is the sound velocity (subscript i represents the P wave or S wave), $\Delta\omega_i$ is
84 the measured Brillouin shift, λ represents the incident wavelength, and θ represents
85 the angle between the incident and scattered orientations.

86 **Results and discussion**

87 **Sound velocities and elastic properties of calcite at high-pressure**

88 The sound velocities of calcite were determined up to 10.3 GPa at ambient
89 temperature in a 0.3-3 GPa pressure interval by Brillouin scattering spectroscopy. The
90 19 sets of Brillouin scattering spectra were collected in the $(10\bar{1}1)$ plane, with 10°
91 intervals for each pressure. The intensities of the compressional wave velocity (V_p)
92 and shear wave velocity (V_s) varied with crystallographic direction. A representative
93 Brillouin scattering spectrum for single-crystal calcite at 1.8 GPa and 300 K is shown
94 in Figure 1. Although calcite has the property of birefringence, given the experimental
95 uncertainty, its effect on velocity can be neglected based on the analysis in a previous
96 study (Chen et al. 2001).

97 The V_p and V_s velocities of single-crystal calcite as a function of the azimuthal
98 angle measured from the $(10\bar{1}1)$ cleaved plane at 0.3 GPa, 1.8 GPa, and 10.3 GPa are

99 shown in Figure 2. The V_p and V_s values varied significantly as a function of the
100 azimuthal angle at each pressure, indicating strong elastic anisotropies of the mineral
101 at different phases. However, the change trends of these velocities were obviously
102 different from each other. A comparison of the velocities at 0.3 and 1.8 GPa reveals
103 that the latter velocities were obviously less than the former velocities. The abnormal
104 decrease in the V_p and V_s velocities at 1.8 GPa corresponded to a different structure
105 of calcite (i.e., $\text{CaCO}_3\text{-II}$ ($P2_1/c$)) (Merrill and Bassett 1975). Furthermore, the change
106 trends of the velocities at 1.8 GPa and 10.3 GPa were obviously different, especially
107 for V_p . At 10.3 GPa, the V_p value strictly varied as a sine or cosine trend with the
108 azimuthal angle, which corresponded to the $\text{CaCO}_3\text{-III}$ phase, and it crystallized in the
109 triclinic space group $P\bar{1}$ (Merlini et al. 2012).

110 Based on the density and 19 sets of velocity data for the calcite at each pressure, the
111 six elastic constants of calcite were calculated by a genetic algorithm using the
112 Christoffel's equations (Chen et al. 2006; Redfern and Angel 1999). This method has
113 been successfully used to calculate the elastic constants of magnesite, dolomite, $\text{Zn}(2\text{-}$
114 $\text{methylimidazolates})_2$ (Chen et al. 2006; Tan et al. 2012), and rhodochrosite (Zhao et al.
115 2018). The error for each elastic constant is estimated by calculating the variations of
116 misfit as a function of the specific C_{ij} (Chen et al. 2006).

117 The adiabatic bulk and shear moduli (K_s and G), were calculated by the Voigt-
118 Reuss-Hill averages (Meister and Peselnick 1966) using the derived elastic constants.
119 The derived bulk and shear moduli (K_0 and G_0) under ambient conditions were 78.2
120 and 32.6 GPa, respectively, which were in agreement with previous results (see Table
121 S1) (Chen et al. 2001; Lin 2013). Then the aggregate V_p and V_s were calculated by
122 the following equations:

$$V_p = \sqrt{\frac{K_s + \frac{4}{3}G}{\rho}}, \quad (2)$$

$$V_s = \sqrt{\frac{G}{\rho}}, \quad (3)$$

123

124

125 The elastic constants and aggregate sound velocity properties of calcite in the form of
126 CaCO₃-I at high-pressure are shown in Table 1. The monoclinic structure of CaCO₃-II
127 and the triclinic structure of CaCO₃-III have thirteen and twenty-one independent
128 elastic constants, respectively, which are difficult to accurately calculate by the
129 genetic algorithm method. This method is better used to calculate the elastic constants
130 in orthorhombic and higher symmetry crystals.

131 To characterize the change trends of the velocities, as a reference, a simple average
132 of the 19 sets of velocities at each pressure was taken as the average velocity of the
133 calcite, as shown in Figure 3. A large discrepancy (~0.6 km/s) was apparent between
134 the aggregate V_p and average V_p values in the CaCO₃-I phase, while a smaller
135 difference was observed between the aggregate V_s and average V_s values. Dramatic
136 decreases in V_p (-16.0%) and V_s (-18.9%) were detected across the phase transition
137 from CaCO₃-I to CaCO₃-II, while dramatic increases in V_p (+6.6%) and V_s (+20.2%)
138 were detected across the phase transition from CaCO₃-II to CaCO₃-III. Sharp
139 decreases in all elastic constants and the bulk modulus of calcite were reported to
140 occur in the phase transition from CaCO₃-I to CaCO₃-II based on ultrasonic
141 interferometry (Thanh and Lacam 1984; Singh and Kennedy 1974). The V_p decrease
142 (-16.0%) across the phase transition from CaCO₃-I to CaCO₃-II in this study is in
143 good agreement with the value of -19.0% reported based on ultrasonic interferometry
144 (Wang 1966), although there is an obvious velocity discrepancy between these two
145 methods. The average velocities measured in this study are almost identical to the

146 values obtained via theoretical calculation (Marcondes et al. 2016). To some extent,
147 the change trends of the average velocities can represent the aggregate velocities. The
148 approximate aggregate Vp and Vs values of CaCO₃-II were calculated based on this
149 assumption.

150 The anisotropy factors for Vp and Vs are defined as follows:

151
$$A_p = 2 \times (V_{P,\max} - V_{P,\min}) / (V_{P,\max} + V_{P,\min}) \times 100\% , \quad (4)$$

152
$$A_s = (V_{s2} - V_{s1}) / V_s \times 100\% , \quad (5)$$

153 where Vp,max and Vp,min represent the maximum and minimum Vp values of the
154 mineral, respectively; Vs1 and Vs2 are two orthogonally polarized Vs values; and Vs
155 represents the aggregate Vs value. The anisotropy factors of Ap and Asmax of calcite
156 are a function of pressure and are shown in Figure 4. The extrapolated Ap and Asmax
157 values are 24.3% and 61.4%, respectively, under ambient conditions, and these values
158 are consistent with those in a previous study (Chen et al. 2001). The anisotropies of
159 calcite in the different phases were considerably different, and the Ap and Asmax of
160 CaCO₃-II were much larger than those of CaCO₃-I and CaCO₃-III. Similarly, a
161 theoretical analysis implies that there are considerable differences in the anisotropies
162 of different phases of CaCO₃ (Marcondes et al. 2016, Huang et al. 2017). The Ap and
163 Asmax were generally stable at ~23% and ~62% in the structure of CaCO₃-I,
164 respectively. Abrupt increases in Ap (+40.9%) and Asmax (+58.4%) were detected
165 across the phase transition from CaCO₃-I to CaCO₃-II. Within CaCO₃-II, the Ap
166 ranged from 31.3% to 32.0%, and Asmax ranged from 76.2% to 96.8%. Furthermore,
167 across the phase transition from CaCO₃-II to CaCO₃-III, an abrupt decrease in Ap (-
168 65.0%) was detected, and the Ap subsequently increased slowly to the maximum
169 pressure in this study.

170 **Phase diagram of CaCO₃**

171 Because the phase diagram of CaCO_3 is fairly complicated and phase transitions are
172 strongly dependent on temperature, the elastic properties of calcite at ambient
173 temperature and high-pressure are carefully applied under high-temperature and high-
174 pressure conditions. To further discuss the geophysical implications of a suitable
175 pressure range, we constructed a phase diagram of CaCO_3 with showing estimated
176 temperature and pressure conditions corresponding to relatively cold subduction zone
177 based on the literature (Figure S1). According to synthesized phase diagram, calcite
178 phases of CaCO_3 -I, CaCO_3 -II and aragonite should be stable in the cold subduction
179 zone beneath NE Japan and Izu-Bonin (Figure S1). Raman spectroscopy in the calcite
180 phases showed that CaCO_3 -II is stable between 1.4 and 2.1 GPa at ambient
181 temperature (Figure S2). This is consistent with the previous studies using Raman
182 spectroscopy and X-ray diffraction measurements (Merlini et al. 2012; Hagiya et al.
183 2005; Liu et al. 2016; Bayarjargal et al. 2018). However, the stability field of CaCO_3 -
184 II should be slightly smaller at higher temperatures because of the negative Clausius-
185 Clapeyron slopes of the phase boundary lines from CaCO_3 -I to CaCO_3 -II and from
186 CaCO_3 -II to aragonite (Pippinger et al. 2015, Liu et al. 2017). For the temperature and
187 pressure conditions of the Izu-Bonin and NE Japan regions, CaCO_3 -II is stable at
188 pressures below ~ 1.7 GPa corresponding to 51 km depth, and then it transforms into
189 aragonite at greater pressures. In contrast, CaCO_3 -III may not exist under the relevant
190 temperature and pressure conditions of the subduction zone beneath NE Japan and
191 Izu-Bonin, since CaCO_3 -III is stable at very low temperature condition. Accordingly,
192 we will focus on the velocities of CaCO_3 -I, CaCO_3 -II and aragonite phases in the
193 upcoming discussion.

194 **Velocities and anisotropies of CaCO_3 and major upper mantle minerals at high-**
195 **pressure**

196 The velocities and anisotropies of CaCO₃ and major upper mantle minerals are
197 shown as a function of pressure in Figure 5. Comparisons are limited to room
198 temperature and high-pressure due to limited knowledge in the temperature effects on
199 the elastic properties of CaCO₃. Combined with the elastic properties of aragonite
200 reported previously (Huang et al. 2017; Liu et al. 2005; Marcondes et al. 2016),
201 CaCO₃ polymorphs have the lowest V_p and V_s values and the largest A_p and A_{smax}
202 values among the major upper mantle minerals over the entire pressure range (see
203 Figure 5).

204 **Velocities of the carbonated eclogite and peridotite models**

205 To further evaluate the effect of carbonate on the velocity of the major upper
206 mantle minerals, we calculated the velocities of eclogite and peridotite with and
207 without 10 wt.% CaCO₃ as reported previously (Bayarjargal et al. 2018). In terms of
208 mineral assemblage, the carbon-free eclogite model is 53.3 wt.% garnet and 46.7 wt.%
209 clinopyroxene, while the carbon-free peridotite model is 59.3 wt.% olivine, 12.8 wt.%
210 clinopyroxene, 11.4 wt.% orthopyroxene, and 16.5 wt.% garnet (Dasgupta and
211 Hirschmann 2006; Dasgupta et al. 2004; Yang et al. 2014). Here we modeled
212 velocities of hypothetical CaCO₃-rich mantle rocks, which are constructed by 90 wt.%
213 of eclogite/peridotite and 10 wt.% of CaCO₃. Compared to the carbon-free eclogite,
214 the V_p and V_s values decrease by 2.3% and 3.0% for CaCO₃-I, 3.6% and 4.4% for
215 CaCO₃-II, and 2.7% and 3.0% for aragonite, respectively. Velocities significantly
216 increase (V_p +1.3 % and V_s +1.4 %) during phase transition from CaCO₃-I to CaCO₃-
217 II. Similarly, the V_p and V_s values of the carbonated peridotite decrease by about 2-4 %
218 compared to normal peridotite (see Figure 6).

219 **Implications**

220 Discontinuities in seismic wave velocities are closely related to phase transitions,

221 rapid variations in chemical composition with depth, or changes in the degree of
222 anisotropy (Stixrude 2015). Sharp increases in V_p (+2%) and V_s (+9%) from
223 aragonite to CaCO_3 -VII at 25 GPa (~690 km depth) and decreases in V_p (-12%) and
224 V_s (-3%) from CaCO_3 -VII to post-aragonite at 40 GPa (~1010 km depth) were
225 previously determined based on density functional theory calculations (Bayarjargal et
226 al. 2018). According to previous study (Bayarjargal et al. 2018), seismic wave
227 velocities increase (V_p +0.4% and V_s +0.9%) upon aragonite to CaCO_3 -VII phase
228 transition at 25 GPa in pyrolite with 10 wt.% of CaCO_3 , while these values largely
229 decrease (V_p -4.7% and V_s -7.0%) during CaCO_3 -VII to post-aragonite transition at
230 40 GPa. These data imply that the presence of CaCO_3 may contribute to the
231 discontinuities at ~700 km and 930-1120 km (Bayarjargal et al. 2018; Yang and He
232 2015; Kaneshima 2013).

233 In this study, we measured the elastic properties of calcite at pressures up to 10.3
234 GPa and observed dramatic decreases in V_p (-16.0%) and V_s (-18.9%) across the
235 phase transition from CaCO_3 -I to CaCO_3 -II, which occurred at ~1.4 GPa (42 km
236 depth). If eclogite or pyrolite contain 10 wt.% of CaCO_3 , seismic wave velocities
237 significantly decrease by V_p -1.3% and V_s -1.4% upon the phase transition at 42 km
238 depth (Figure 6). The sharp decreases in the V_p and V_s values of CaCO_3 across the
239 phase transition may be related to the Gutenberg discontinuity at ~51(\pm 10) km, where
240 the V_s changes by -7.8%, as reported by seismic observations in the Izu-Bonin region
241 (Revenaugh and Jordan 1991). On the other hand, we observed abrupt increases in A_p
242 (+40.9%) and A_{max} (+58.4%) across the phase transition. A small amount of calcite-
243 type carbonates can significantly modify the seismic anisotropy of rocks (Valcke et al.
244 2006; Lin 2013). A strong, localized anisotropy is also considered to explain the
245 Gutenberg discontinuity (Stixrude 2015; Gung et al. 2003). If calcite exists in the Izu-

246 Bonin region in a sufficient quantity, the phase transition from CaCO₃-I to CaCO₃-II
247 may represent a possible explanation of the Gutenberg discontinuity at 51 km in this
248 region.

249 A low-velocity layer has been observed in NE Japan, and it extends to 150 km
250 depth beneath this region (Peacock 2003; Matsuzawa et al. 1986; Hasegawa et al.
251 1994). Under the relevant temperature and pressure conditions of the NE Japan region,
252 the velocities of CaCO₃, including CaCO₃-I, CaCO₃-II, and aragonite, are much
253 slower than those of the major upper mantle minerals up to at least 10 GPa (300 km
254 depth) (see Figure 5 (a), (b)). As described above, we estimated sound wave velocities
255 of mantle rocks (eclogite and peridotite) containing 10 wt.% of CaCO₃ (Figure 6).
256 Results show that velocities significantly reduced by enrichment of CaCO₃ up to -4.4%
257 compared to normal mantle. The presence of CaCO₃ at relevant depths in the NE
258 Japan region may potentially explain the low-velocity zone observed in this region. In
259 addition, a previous study suggested that the sound velocities of CaCO₃ in the post-
260 aragonite phase were much lower than those of the major lower mantle constituent
261 MgSiO₃, and the presence of CaCO₃ was considered a possible way to explain the
262 existence of the low-velocity region in the bottom of the lower mantle (Marcondes et
263 al. 2016). The rather low velocities and large anisotropies of carbonates (see Figure
264 S3 and reference in (Marcondes et al. 2016)) can be considered potentially useful
265 features for detecting carbonate-rich regions in the Earth's crust and mantle, which
266 further improve our knowledge of the deep carbon cycle and seismic observations in
267 the Earth's interior.

268 **Acknowledgments**

269 We very appreciated two anonymous reviewers and editors for their suggestions and
270 comments, which greatly improved the manuscript. We acknowledged Changsheng

271 Zha for the guidance and advice on the experiment. We also thanked Wenqiang Yang
272 for the help of electron microprobe measurements. This work was supported by the
273 Strategic Priority Research Program (B) of the Chinese Academy of Sciences under
274 Grant XDB18010401 and Major State Research Development Program of China
275 under Grant 2016YFC0601101.

276 **References**

- 277 Almqvist, B.S.G., Burlini, L., Mainprice, D., and Hirt, A.M. (2010) Elastic properties
278 of anisotropic synthetic calcite-muscovite aggregates. *Journal of Geophysical*
279 *Research*, 115, B08203.
- 280 Bayarjargal, L., Fruhner, C.-J., Schrodt, N., Winkler, B. (2018) CaCO₃ phase
281 diagram studied with Raman spectroscopy at pressures up to 50 GPa and high-
282 temperatures and DFT modeling. *Physics of the Earth and Planetary Interiors*,
283 281, 31–45.
- 284 Brenker, F.E., Vollmer, C., Vincze, L., Vekemans, B., Szymanski, A., Janssens, K.,
285 Szaloki, I., Nasdala, L., Joswig, W., and Kaminsky, F. (2007) Carbonates from
286 the lower part of transition zone or even the lower mantle. *Earth and Planetary*
287 *Science Letters*, 260, 1–9.
- 288 Catalli, K. (2005) A high-pressure phase transition of calcite-III. *American*
289 *Mineralogist*, 90, 1679–1682.
- 290 Chai, M., Brown, J.M., and Slutsky, L.J. (1997) The elastic constants of an aluminous
291 orthopyroxene to 12.5 GPa. *Journal of Geophysical Research*, 102, 14779–
292 14785.
- 293 Chen, C.-C., Lin, C.-C., Liu, L.-G., Sinogeikin, S.V. and Bass, J.D. (2001) Elasticity
294 of single-crystal calcite and rhodochrosite by Brillouin spectroscopy.
295 *American Mineralogist*, 86, 1525–1529.

- 296 Chen, P.-F., Chiao, L.-Y., Huang, P.-H., Yang, Y.-J., and Liu, L.-G. (2006) Elasticity
297 of magnesite and dolomite from a genetic algorithm for inverting Brillouin
298 spectroscopy measurements. *Physics of the Earth and Planetary Interiors*, 155,
299 73–86.
- 300 Collins, M.D., and Brown, J.M. (1998) Elasticity of an upper mantle clinopyroxene.
301 *Physics and Chemistry of Minerals*, 26, 7-13.
- 302 Dasgupta, R., and Hirschmann, M.M. (2006) Melting in the Earth's deep upper mantle
303 caused by carbon dioxide. *Nature*, 440(7084), 659-662.
- 304 Dasgupta, R., and Hirschmann, M.M. (2010) The deep carbon cycle and melting in
305 Earth's interior. *Earth and Planetary Science Letters*, 298, 1–13.
- 306 Dasgupta, R., Hirschmann, M.M., and Withers, A.C. (2004) Deep global cycling of
307 carbon constrained by the solidus of anhydrous, carbonated eclogite under
308 upper mantle conditions. *Earth and Planetary Science Letters*, 227(1-2), 73-85.
- 309 Dorfman, S.M., Badro, J., Nabiei, F., Prakapenka, V.B., Cantoni, M., and Gillet, P.
310 (2018) Carbonate stability in the reduced lower mantle. *Earth and Planetary
311 Science Letters*, 489, 84–91.
- 312 Duffy, T.S., and Anderson, D.L. (1989) Seismic velocities in mantle minerals and the
313 mineralogy of the upper mantle. *Journal of Geophysical Research*, 94(B2),
314 1895-1912.
- 315 Duffy, T.S., Zha, C.-S., Downs, R.T., Mao, H.-K., Hemley, R.J. (1995) Elasticity of
316 forsterite to 16 GPa and the composition of the upper mantle. *Nature Letters*,
317 278, 170–173.
- 318 Grady, D.E., Hollenbach, R.E., and Schuler, K.W. (1978) Compression wave studies
319 on calcite rock. *Journal of Geophysical Research*, 83, 2839–2849.
- 320 Gung, Y.C., Panning, M., Romanowicz, B. (2003) Dissociative hydrogen adsorption

- 321 on palladium requires aggregates of three or more vacancies. *Nature*, 422
322 (6933), 705–707.
- 323 Hagiya, K., Matsui, M., Kimura, Y. and Akahama, Y. (2005) The crystal data and
324 stability of calcite III at high-pressures based on single-crystal X-ray
325 experiments. *Journal of Mineralogical and Petrological Sciences*, 100, 31–36.
- 326 Hasegawa, A., Horiuchi, S. and Umino, N. (1994) Seismic structure of the
327 northeastern Japan convergent plate margin: A synthesis, *Journal of*
328 *Geophysical Research*, 99(22), 22295-22311.
- 329 Huang, D., Liu, H., Hou, M.-Q., Xie, M.-Y., Lu, Y.-F., Liu, L., Yi, L., Cui, Y.-J., Li,
330 Y., Deng, L.-W., and Du, J.-G. (2017) Elastic properties of CaCO₃ high-
331 pressure phases from first principles. *Chinese Physics B*, 26, 089101.
- 332 Juneja, A., and Endait, M. (2017) Laboratory measurement of elastic waves in Basalt
333 rock. *Measurement*, 103, 217–226.
- 334 Kaminsky, F., Wirth, R., Matsyuk, S., Schreiber, A., and Thomas, R. (2009)
335 Nyerereite and nahcolite inclusions in diamond: evidence for lower-mantle
336 carbonatitic magmas. *Mineralogical Magazine*, 73, 797–816.
- 337 Kaneshima, S., 2013. Lower mantle seismic scatterers below the subducting Tonga
338 slab: evidence for slab entrainment of transition zone materials. *Physics of the*
339 *Earth and Planetary Interiors*, 222, 35–46.
- 340 Li, X.-Y., Zhang, Z.-G, Lin, J.-F., Ni, H.-W., Prakapenka, V.B., and Mao, Z. (2018)
341 New high-pressure phase of CaCO₃ at the topmost lower mantle implication
342 for the deep-mantle carbon transportation. *Geophysical Research Letters*, 45,
343 1355–1360.
- 344 Lin, C.-C. (2013) Elasticity of calcite: thermal evolution. *Physics and Chemistry of*
345 *Minerals*, 40, 157–166.

- 346 Liu, J., Caracas, R., Fan, D.-W., Bobocioiu, E., Zhang, D., and Mao, W.L. (2016)
347 High-pressure compressibility and vibrational properties of (Ca,Mn)CO₃.
348 American Mineralogist, 101, 2723–2730.
- 349 Liu, L.-G., Chen, C.-C., Lin, C.-C., and Yang, Y.-J. (2005) Elasticity of single-crystal
350 aragonite by Brillouin spectroscopy. Physics and Chemistry of Minerals, 32(2),
351 97-102.
- 352 Lu, C., Mao, Z., Lin, J.-F., Zhuravlev, K.K., Tkachev, S.N., and Prakapenka, V.B.
353 (2013) Elasticity of single-crystal iron-bearing pyrope up to 20 GPa and 750 K.
354 Earth and Planetary Science Letters, 361, 134–142.
- 355 Mao, H.-K., Xu, J.-A., Bell, P.M. (1986) Calibration of the ruby pressure gauge to
356 800 kbar under quasi-hydrostatic conditions. Journal of Geophysical Research,
357 91, 4673–4676.
- 358 Mao, Z., Fan, D.-W., Lin, J.-F., Yang, J., Tkachev, S.N., Zhuravlev, K., and Prakape-
359 nka, V.B. (2015) Elasticity of single-crystal olivine at high-pressures and tem-
360 peratures. Earth and Planetary Science Letters, 426, 204-215.
- 361 Mao, Z., Jacobsen, S.D., Jiang, F., Smyth, J.R., Holl, C.M., Frost, D.J., and Duffy,
362 T.S. (2010) Velocity crossover between hydrous and anhydrous forsterite at
363 high-pressures. Earth and Planetary Science Letters, 293, 250–258.
- 364 Marcondes, M.L., Justo, J.F., and Assali, L.V.C. (2016) Carbonates at high-pressures
365 Possible carriers for deep carbon reservoirs in the Earth's lower mantle.
366 Physical Review B, 94, 104112.
- 367 Matsuzawa, T., Umino, N., Hasegawa, A., and Takagi, A. (1986) Upper mantle
368 velocity structure estimated from PS-converted wave beneath the northeastern
369 Japan Arc. Geophysical Journal Royal Astronomical Society, 86, 767-787.
- 370 Meister, R., and Peselnick, L. (1966) Variational method of determining effective

- 371 moduli of polycrystals with tetragonal symmetry. *Journal of Applied Physics*,
372 37, 4121–4125.
- 373 Merlini, M., Hanfland, M., and Crichton, W.A. (2012) CaCO₃-III and CaCO₃-VI,
374 high-pressure polymorphs of calcite: Possible host structures for carbon in the
375 Earth's mantle. *Earth and Planetary Science Letters*, 333–334, 265–271.
- 376 Merrill, B.L., and Bassett, W.A. (1975) The crystal structure of CaCO₃(II), a high-
377 pressure metastable phase of calcium carbonate. *Acta Crystallographica*, B31,
378 343–349.
- 379 Oganov, A.R., Glass, C.W., and Ono, S. (2006) High-pressure phases of CaCO₃:
380 Crys-tal structure prediction and experiment. *Earth and Planetary Science*
381 *Letters*, 241, 95–103.
- 382 Oganov, A.R., Ono, S., Ma, Y., Glass, C.W., and Garcia, A. (2008) Novel high-
383 pressure structures of MgCO₃, CaCO₃ and CO₂ and their role in Earth's lower
384 mantle. *Earth and Planetary Science Letters*, 273, 38–47.
- 385 Ono, S., Kikegawa, T., and Ohishi, Y. (2007) High-pressure transition of CaCO₃.
386 *American Mineralogist*, 92, 1246–1249.
- 387 Peacock, S.M. (2003) Thermal structure and metamorphic evolution of subducting
388 slabs. In J.M. Eiler Eds., *Inside the Subduction Factory*, Geophysical
389 Monograph, p. 7–22. AGU Press, Washington, D.C.
- 390 Peselnick, L., and Robie, R.A. (1963) Elastic Constants of Calcite. *Journal of Applied*
391 *Physics*, 34, 2494–2495.
- 392 Pippinger, T., Miletich, R., Merlini, M., Lotti, P., Schouwink, P., Yagi, T., Crichton,
393 W.A., and Hanfland, M. (2015) Puzzling calcite-III dimorphism:
394 crystallography, high-pressure behavior, and pathway of single-crystal
395 transitions. *Physics and Chemistry of Minerals*, 42, 29–43.

- 396 Redfern, S.A.T., and Angel, R.J. (1999) High-pressure behaviour and equation of
397 state of calcite, CaCO₃. Contributions to Mineralogy and Petrology, 134, 102–
398 106.
- 399 Sanchez-Valle, C., Ghosh, S., and Rosa, A.D. (2011) Sound velocities of ferromag-
400 nesian carbonates and the seismic detection of carbonates in eclogites and the
401 mantle. Geophysical Research Letters, 38, L24315.
- 402 Sanchez-Valle, C., Mantegazzi, D., Bass, J.D., and Reusser, E. (2013) Equation of
403 state, refractive index and polarizability of compressed water to 7 GPa and
404 673 K. Journal of Chemical Physics, 138, 054505.
- 405 Sang, L.-Q., and Bass, J.D. (2014) Single-crystal elasticity of diopside to 14 GPa by
406 Brillouin scattering. Physics of the Earth and Planetary Interiors, 228, 75–79.
- 407 Singh, A.K., and Kennedy, G.C. (1974) Compression of calcite to 40 kbar. Journal of
408 Geophysical Research, 79, 2615–2622.
- 409 Sinogeikin, S.V., and Bass, J.D. (2000) Single-crystal elasticity of pyrope and MgO to
410 20 GPa by Brillouin scattering in the diamond cell. Physics of the Earth and
411 Planetary Interiors, 120, 43-62.
- 412 Stekiel, M., Nguyen-Thanh, T., Chariton, S., McCammon, C., Bosak, A., Morgenroth,
413 W., Milman, V., Refson, K., and Winkler, B. (2017) High-pressure elasticity
414 of FeCO₃-MgCO₃ carbonates. Physics of the Earth and Planetary Interiors,
415 271, 57–63.
- 416 Stixrude, L. (2005) Mineralogy and elasticity of the oceanic upper mantle: Origin of
417 the low-velocity zone. Journal of Geophysical Research, 110, B03204.
- 418 Stixrude, L. (2015) Properties of rocks and minerals—seismic properties of rocks and
419 minerals, and structure of the Earth. In A. Dziewonski and B. Romanowicz,
420 Eds., Treatise on Geophysics: Mineral Physics, 2ed. p. 417–421. Elsevier.

- 421 Tan, J.-C., Civalleri, B., Lin, C.-C., Valenzano, L., Galvelis, R., Chen, P.-F., Bennett,
422 T.D., Mellot-Draznieks, C., Zicovich-Wilson, C.M., and Cheetham, A.K.
423 (2012) Exceptionally low shear modulus in a prototypical imidazole-based
424 metal-organic framework. *Physical Review Letters*, 108, 095502.
- 425 Thanh, D.V., and Lacam, A. (1984) Experimental study of the elasticity of single
426 crystalline calcite under high-pressure (the calcite I-calcite II transition at 14.6
427 kbar). *Physics of the Earth and Planetary Interiors*, 34, 195–203.
- 428 Tschauner, O., Huang, S., Greenberg, E., Prakapenka, V. B., Ma, C., Rossman, G.R.,
429 Shen, A.H., Zhang, D., Newville, M., Lanzirotti, A., Tait, K. (2018) Ice-VII
430 inclusions in diamonds Evidence for aqueous fluid in Earth’s deep mantle.
431 *Science*, 359, 1136–1139.
- 432 Wang, C.-Y. (1966) Velocity of compression waves in limestones, marbles, and a
433 Single-crystal of calcite to 20 Kilobars. *Journal of Geophysical Research*, 71,
434 3543–3547.
- 435 Yang, J., Mao, Z., Lin, J.-F., and Prakapenka, V.B. (2014) Single-crystal elasticity of
436 the deep-mantle magnesite at high-pressure and temperature. *Earth and*
437 *Planetary Science Letters*, 392, 292–299.
- 438 Yang, Z., and He, X., 2015. Oceanic crust in the mid-mantle beneath west-central
439 Pacific subduction zones: evidence from S to P converted waveforms.
440 *Geophysical Journal International*, 203, 541–547.
- 441 Yoneda, A., and Song, M. (2005) Frequency domain analysis of ultrasonic velocity:
442 An alternative bond effect correction constraining bond properties. *Journal of*
443 *Applied Physics*, 97, 024908.
- 444 Zha, C.-S., Duffy, T.S., and Downs, R.T. (1998) Brillouin scattering and X-ray
445 diffraction of San Carlos olivine direct pressure determination to 32 GPa.

- 446 Earth and Planetary Science Letters, 159, 25-33.
- 447 Zhao, C.-S, Li, H.-P, Chen, P.-F, Jiang, J.-J, and Liang, W. (2018) Single-crystal
448 elasticity of the rhodochrosite at high-pressure by Brillouin scattering
449 spectroscopy. High Pressure Research, 10.1080/08957959.2018.1497624.
- 450 Zhao, J., Zhou, B., Liu, B., and Guo, W. (2009) Elasticity of single-crystal calcite by
451 first-principles calculations. Journal of Computational and Theoretical
452 Nanoscience, 6, 1181–1188.
- 453 Zou, F., Wu, Z.-Q., Wang, W.-Z., Wentzcovitch, R.M. (2018) An extended semiana-
454 lytical approach for thermoelasticity of monoclinic crystals: application to
455 diopside. Journal of Geophysical Research: Solid Earth, 10.1029/2018JB016-
456 102.
- 457
- 458
- 459
- 460
- 461
- 462
- 463
- 464
- 465
- 466
- 467
- 468
- 469
- 470
- 471
- 472

473 **Figure captions**

474 **Figure 1.** A representative Brillouin spectrum of single-crystal calcite at 1.8 GPa and
475 300 K. The inserted picture represents the single-crystal calcite in a diamond anvil
476 cell. R: Rayleigh peak. Vp and Vs stand for compressional and transverse velocities.

477 **Figure 2.** Vp and Vs velocities of single-crystal calcite as a function of the azimuthal
478 angle measured from a cleaved (101) platelet. (a) CaCO₃-I, 0.3 GPa; (b) CaCO₃-II,
479 1.8 GPa; (c) CaCO₃-III, 10.3 GPa. The dotted lines represent the change trends of the
480 velocities.

481 **Figure 3.** Vp and Vs velocities of calcite as a function of pressure at ambient
482 temperature. The dashed lines represent the tentative trend of the average sound
483 velocities.

484 **Figure 4.** Ap and Asmax Anisotropies of calcite as a function of pressure at ambient
485 temperature. The dashed lines represent the tentative change trend of the anisotropies.

486 **Figure 5.** Pressure dependence of Vp (a) and Vs (b) velocities and Ap (c) and Asmax
487 (d) anisotropies of CaCO₃ and major upper mantle minerals at 300 K. Black lines:
488 calcite (Cal) (this study; Chen et al. 2001); dark cyan lines: aragonite (Arag) (Huang
489 et al. 2017; Liu et al. 2005; Marcondes et al. 2016); olive lines: olivine (Ol) (Mao et al.
490 2015; Zha et al. 1998); green lines: garnet (Gt) (Duffy and Anderson 1989; Sinogeikin
491 and Bass 2000); wine lines: clinopyroxene (Cpx) (Duffy and Anderson 1989; Sang
492 and Bass 2014; Collins and Brown 1998; Zou et al. 2018); blues lines: orthopyroxene
493 (Opx) (Chai et al. 1997; Duffy and Anderson 1989).

494 **Figure 6.** Vp and Vs velocities of eclogite and peridotite models with and without
495 CaCO₃ at ambient temperature. (a) eclogite model; (b) peridotite model. In terms of
496 mineral assemblage, the carbon-free eclogite model is 53.3 wt.% garnet and 46.7 wt.%
497 clinopyroxene, while the carbon-free peridotite model is 59.3 wt.% olivine, 12.8 wt.%

498 clinopyroxene, 11.4 wt.% orthopyroxene, and 16.5 wt.% garnet (Dasgupta and
499 Hirschmann, 2006; Dasgupta et al. 2004; Yang et al. 2014). The carbonated eclogite
500 and peridotite models include 10 wt.% CaCO₃ (CaCO₃-I, CaCO₃-II, aragonite),
501 respectively.

502

503

504

505

506

507

508

509

510

511

512

513

514

515

516

517

518

519

520

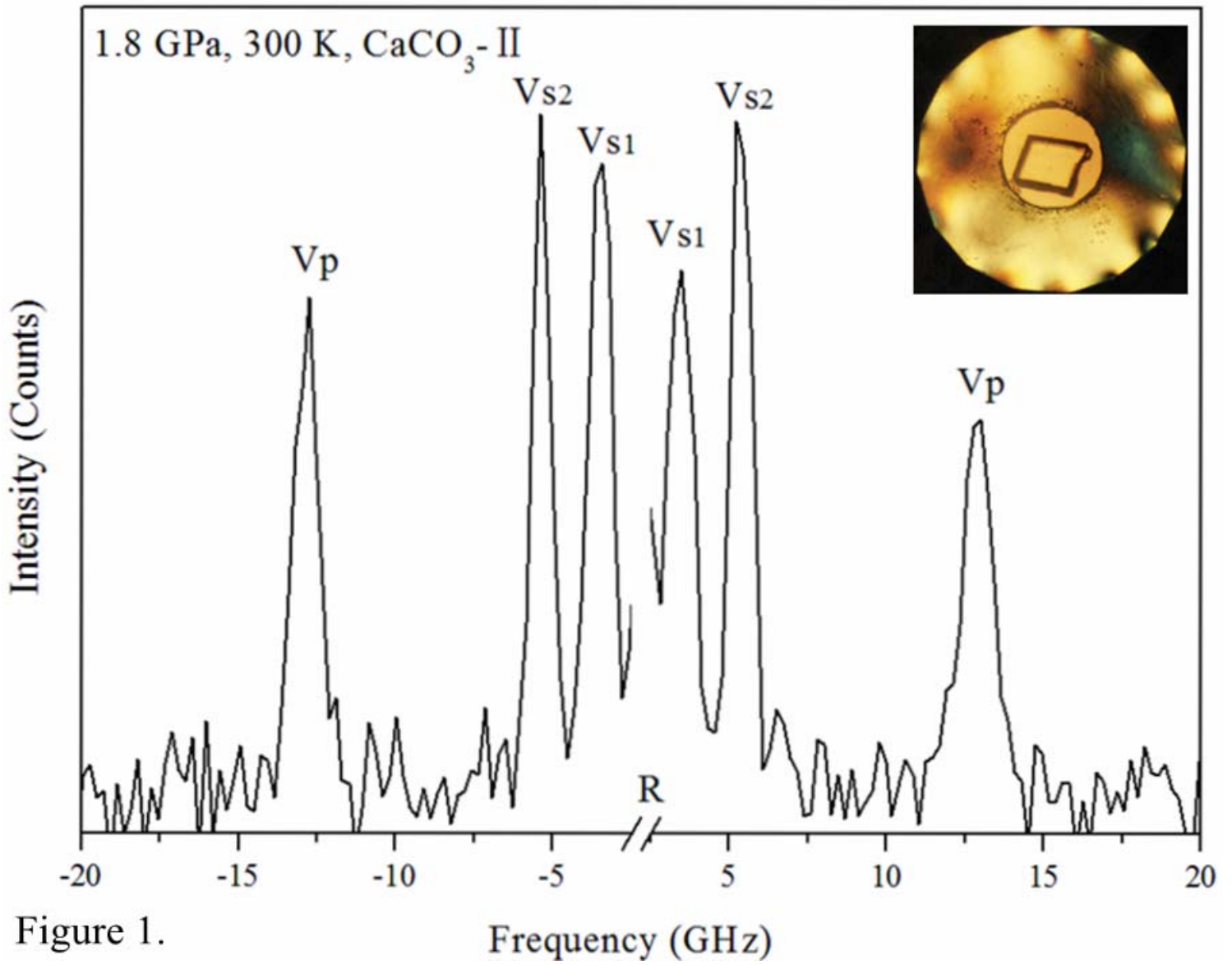
521

522

523 Table 1. Single-crystal elastic properties of calcite in the CaCO₃-I phase under high-
524 pressure and ambient temperature conditions.

P (GPa)	0.3±0.1	0.7±0.1	1.0±0.1	1.3±0.1
C₁₁ (GPa)	150.8±1.5	151.8±1.5	152.5±1.5	153.5±2.0
C₃₃ (GPa)	90.2±3.0	93.9±3.5	93.8±3.5	94.3±4.0
C₄₄ (GPa)	35.4±0.5	39.6±2.0	42.4±1.5	44.9±1.5
C₁₂ (GPa)	63.2±2.5	66.7±2.5	71.2±2.5	73.8±3.0
C₁₃ (GPa)	56.8±1.5	59.2±2.0	61.4±2.5	63.4±2.5
C₁₄ (GPa)	20.0±0.5	20.6±0.5	21.1±0.5	21.7±1.0
K_s (GPa)	79.9±1.7	82.5±1.9	84.3±2.0	85.9±3.1
G (GPa)	32.8±1.6	34.1±2.3	34.1±2.1	34.5±2.5
V_P (km/s)	6.74±0.11	6.84±0.13	6.87±0.13	6.91±0.17
V_S (km/s)	3.47±0.02	3.53±0.03	3.52±0.03	3.54±0.04
A_p (%)	23.1	22.9	23.1	23.7
A_{Smax} (%)	61.5	61.6	61.7	61.2

525



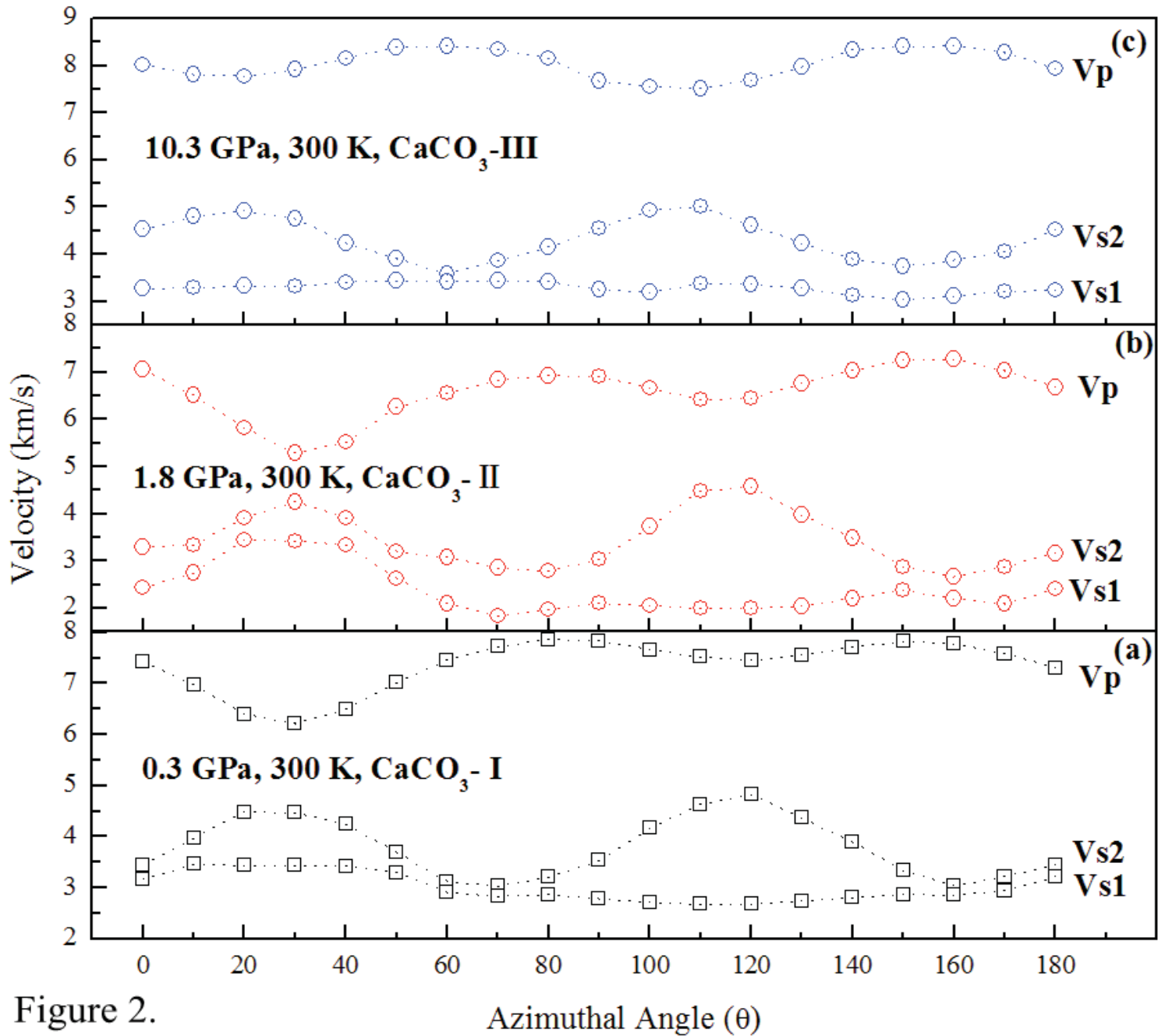


Figure 2.

Azimuthal Angle (θ)

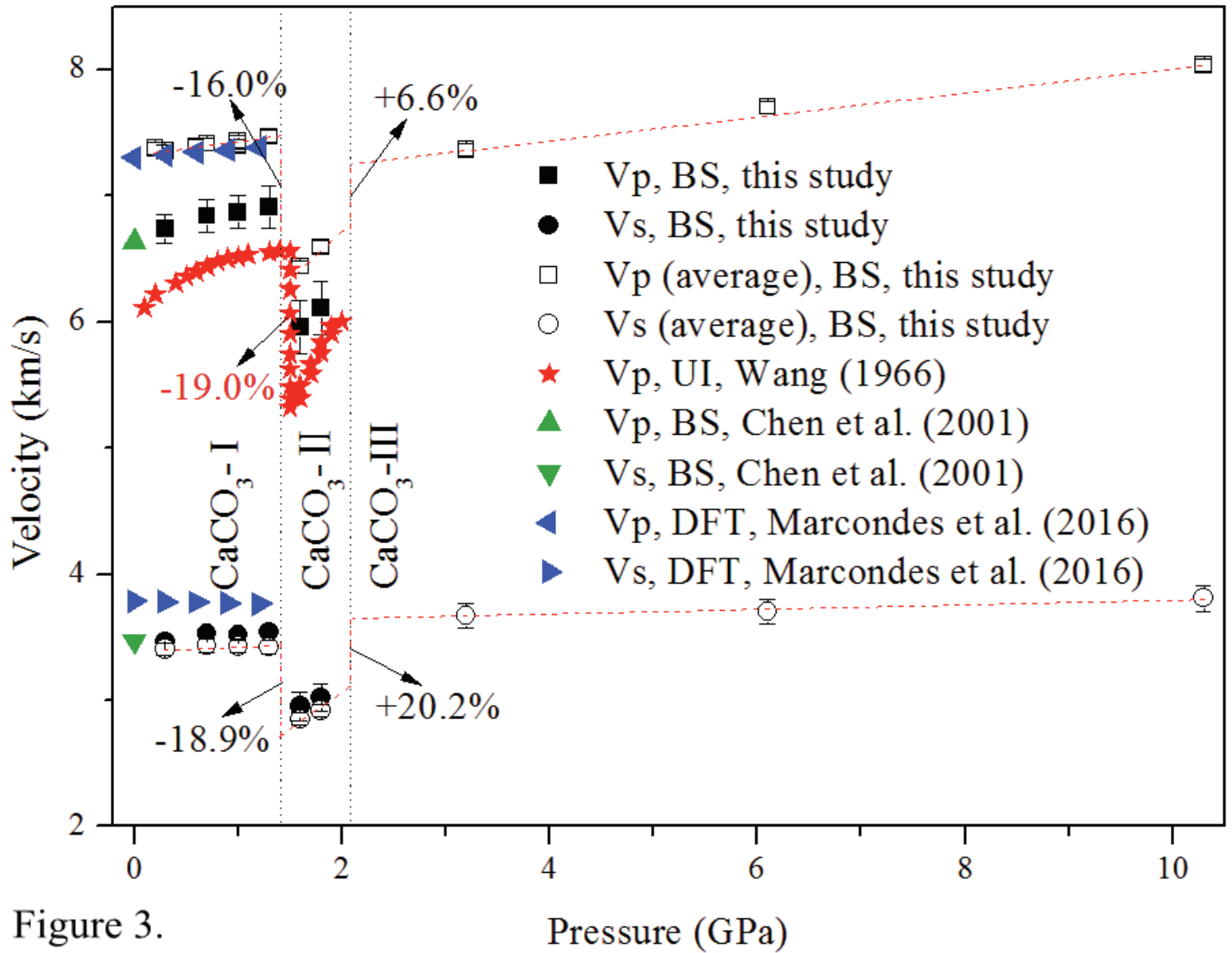


Figure 3.

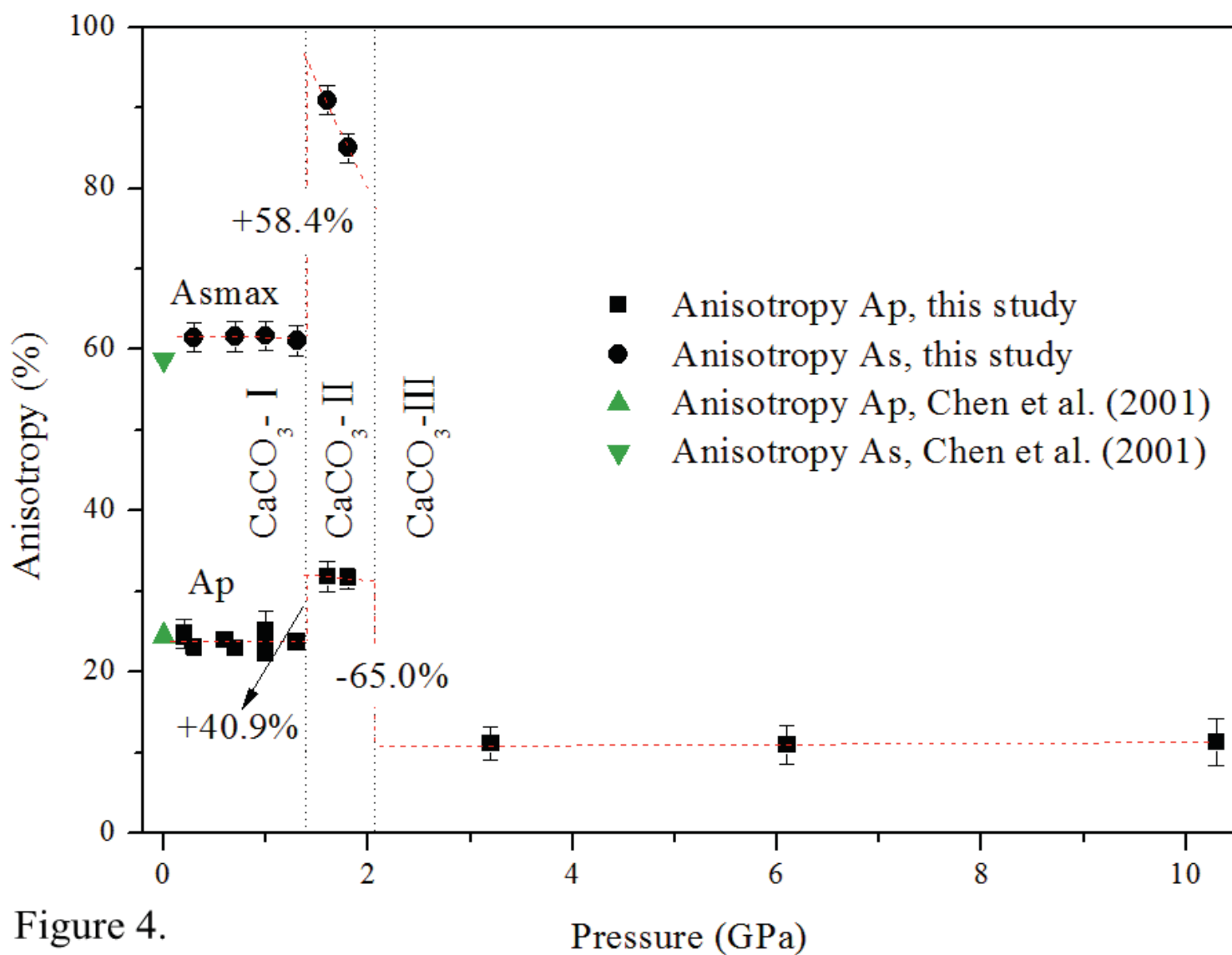


Figure 4.

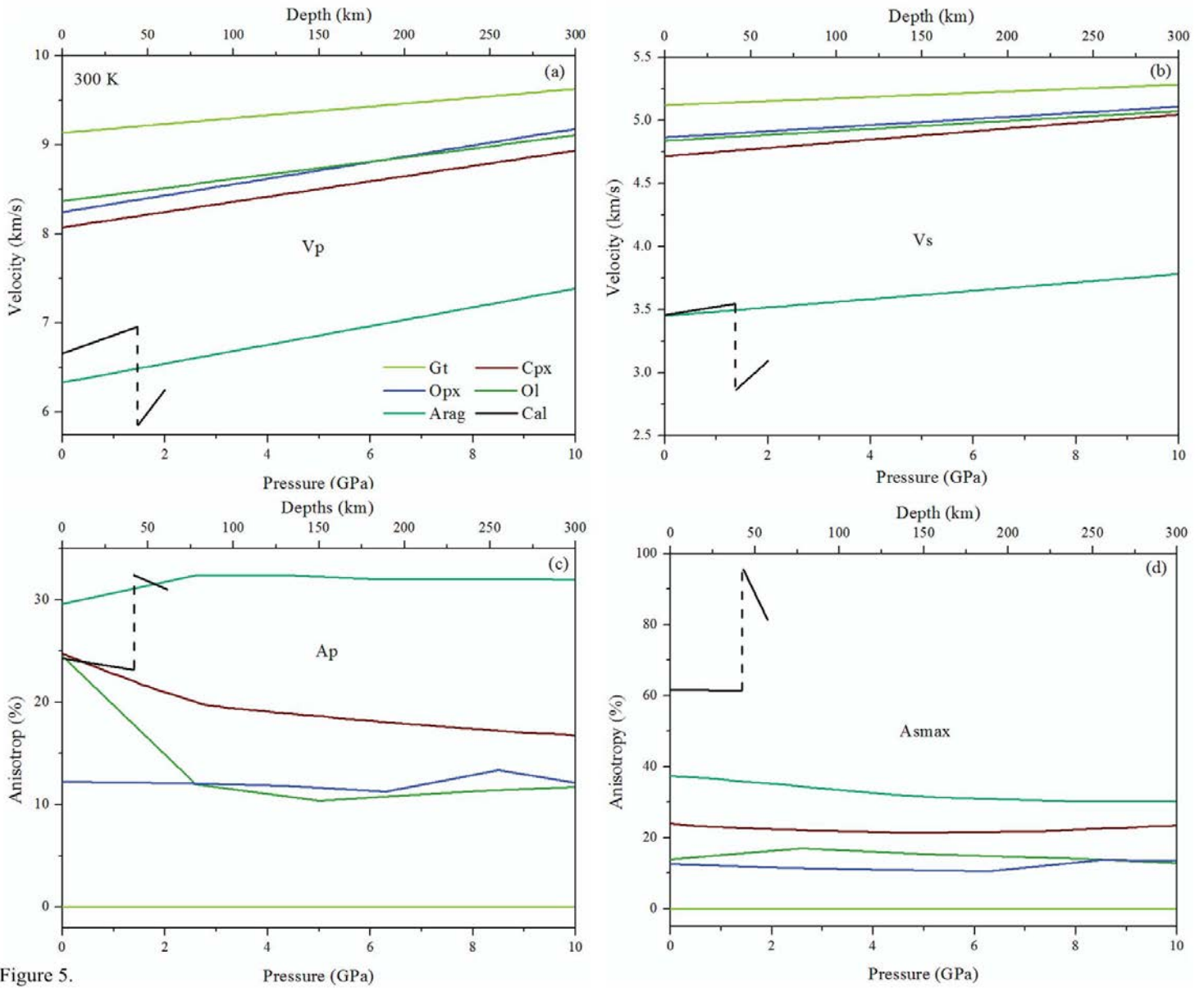


Figure 5.

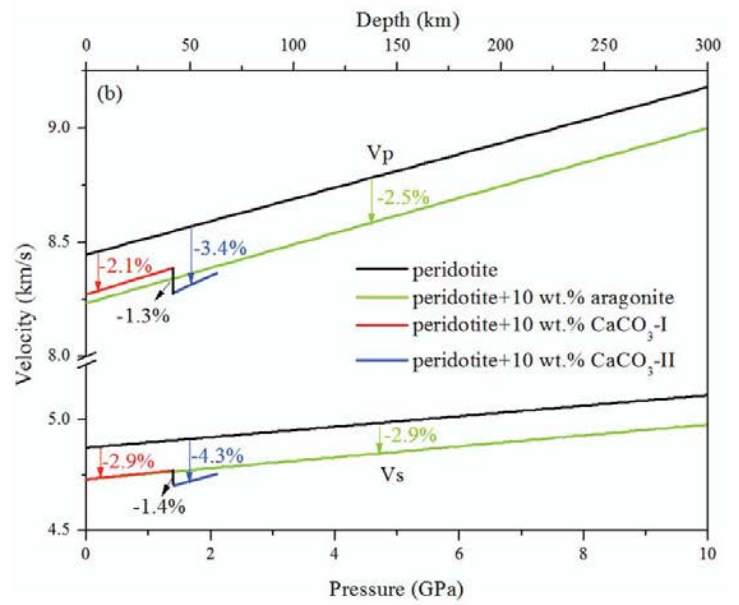
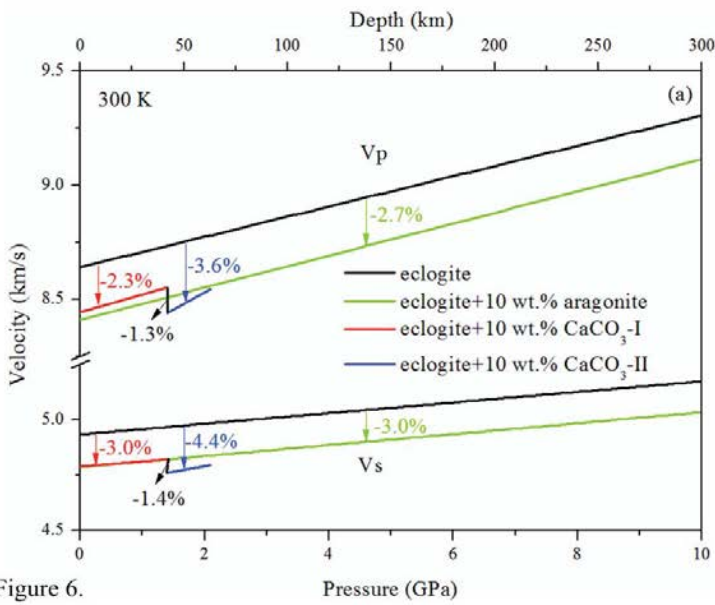


Figure 6.